DOI: 10.1093/jnci/djq153
Advance Access publication on May 18, 2010.

ARTICLE

Effect of the Secretory Small GTPase Rab27B on Breast Cancer Growth, Invasion, and Metastasis

An Hendrix, Dawn Maynard, Patrick Pauwels, Geert Braems, Hannelore Denys, Rudy Van den Broecke, Jo Lambert, Simon Van Belle, Veronique Cocquyt, Christian Gespach, Marc Bracke, Miguel C. Seabra, William A. Gahl, Olivier De Wever, Wendy Westbroek

Manuscript received March 2, 2009; revised March 5, 2010; accepted April 8, 2010.

Correspondence to: Wendy Westbroek, Medical Genetics Branch, National Human Genome Research Institute, 10 Center Dr, Bethesda, MD 20892 (e-mail: wwestbro@mail.nih.gov) or Olivier De Wever, Laboratory of Experimental Cancer Research, Ghent University Hospital, De Pintelaan 185, 9000 Ghent, Belgium (e-mail: olivier.dewever@ugent.be).

Background Secretory GTPases like Rab27B control vesicle exocytosis and deliver critical proinvasive growth regulators into the tumor microenvironment. The expression and role of Rab27B in breast cancer were unknown.

Methods Expression of green fluorescent protein (GFP) fused with wild-type Rab3D, Rab27A, or Rab27B, or Rab27B point mutants defective in GTP/GDP binding or geranylgeranylation, or transient silencing RNA to the same proteins was used to study Rab27B in estrogen receptor (ER)–positive human breast cancer cell lines (MCF-7, T47D, and ZR75.1). Cell cycle progression was evaluated by flow cytometry, western blotting, and measurement of cell proliferation rates, and invasion was assessed using Matrigel and native type I collagen substrates. Orthotopic tumor growth, local invasion, and metastasis were analyzed in mouse xenograft models. Mass spectrometry identified proinvasive growth regulators that were secreted in the presence of Rab27B. Rab27B protein levels were evaluated by immunohistochemistry in 59 clinical breast cancer specimens, and Rab3D, Rab27A, and Rab27B mRNA levels were analyzed by quantitative real-time polymerase chain reaction in 20 specimens. Statistical tests were two-sided.

Results Increased expression of Rab27B promoted G_1 to S phase cell cycle transition, proliferation and invasiveness of cells in culture, and invasive tumor growth and hemorrhagic ascites production in a xenograft mouse model (n = 10; at 10 weeks, survival of MCF-7 GFP- vs GFP-Rab27B–injected mice was 100% vs 62.5%, hazard ratio = 0.26, 95% confidence interval = 0.08 to 0.88, $P = .03$). Mass spectrometric analysis of purified Rab27B-secretory vesicles identified heat-shock protein 90α as key proinvasive growth regulator. Heat-shock protein 90α secretion was Rab27B-dependent and was required for matrix metalloproteinase-2 activation. All Rab27B-mediated functional responses were GTP- and geranylgeranyl-dependent. Presence of endogenous Rab27B mRNA and protein, but not of Rab3D or Rab27A mRNA, was associated with lymph node metastasis ($P < .001$) and differentiation grade ($P = .001$) in ER-positive human breast tumors.

Conclusions Rab27B regulates invasive growth and metastasis in ER-positive breast cancer cell lines, and increased expression is associated with poor prognosis in humans.

J Natl Cancer Inst 2010;102:866–880

Cancers achieve invasive growth by delivering critical factors into the tumor microenvironment (1), but the molecular mechanisms for the secretion of these proinvasive growth regulators remain largely unknown. One likely process involves vesicle exocytosis whose role in tumor progression was first reported by Palmer et al. (2). They showed that ectopic expression of BAIAP3, a Munc 13-like effector of regulated exocytosis, enhanced the malignancy of cancer cells.

Key players in exocytic and endocytic membrane trafficking include the Rab GTPases, which serve as molecular switches that oscillate between active GTP-bound and inactive GDP-bound conformations. Rab GTPases recruit specific protein complexes to elicit their biological functions (3–6); they are posttranslationally modified by geranylgeranylation, which binds them to lipophilic membranes (7).

The secretory pathway can proceed in either a constitutive or a regulated manner (8). In the constitutive pathway, release of vesicle content occurs at a constant rate, and vesicles do not accumulate to an appreciable extent (9). By contrast, regulated secretion involves two distinct steps. Newly synthesized proteins are first stored within vesicular structures and are then released upon stimulation (10). Certain Rab GTPases, referred to as secretory Rabs, control this secretory process; they include Rab26, Rab37, Rab3A/B/C/D, and Rab27A/B (11). Rab26 and Rab37 are thought to modulate secretion in specialized cell types, whereas the Rab3 and Rab27 subfamilies function as more generic regulators of secretion

(12–16). Rab3A/B/C are predominantly expressed in the nervous system, whereas Rab3D and Rab27A/B are present in several nonneuronal secretory tissues and in hematopoietic cells (17). The Rab27 subfamily has the highest homology (41%–44%) to members of the Rab3 subfamily; Rab27A and Rab27B exhibit 71% identity at the amino acid level with each other (18).

Rab proteins of the endocytic pathway (eg, Rab25, Rab13, Rab23, and Rab5) and the constitutive secretory pathway (eg, Rab8) play major roles in malignancy (19–24). Rab GTPases that regulate exocytosis (eg, Rab27A and Rab37) could also be critical for cancer progression (25–27). In this study, we investigated whether aberrant secretory Rab expression contributes to malignancy using silencing or overexpression of each secretory Rab GTPase in estrogen receptor (ER)–positive breast cancer cells in vitro and in vivo. We also examined whether endogenous mRNA and protein levels of secretory Rabs were increased in clinical samples.

CONTEXT AND CAVEATS

Prior knowledge

The Rab27B GTPase has been reported to regulate vesicle exocytosis, but its role in cancer was not clear.

Study design

Wild-type and mutant versions of Rab27B fused to green fluorescent protein were expressed in three estrogen receptor–positive human breast cancer cell lines to determine their effects on cell morphology, proliferation and invasion in culture, and invasive tumor growth in mice. Components of Rab27B-regulated vesicles were identified by mass spectroscopy. Rab27B expression was examined in human breast cancer specimens.

Contribution

Overexpression of Rab27B promoted cell proliferation and invasiveness in vitro and in vivo. Heat-shock protein 90α was a proinvasive component of Rab27B-regulated vesicles. Rab27B was overexpressed in later-stage estrogen receptor–positive breast tumors.

Implications

Inhibitors of Rab27B-regulated pathways may have therapeutic potential.

Limitations

Invasive estrogen receptor–positive human breast cancer cell lines were not available to test the effects of Rab27B silencing RNA, and the mechanism of Rab27B-induced invasiveness has not yet been examined in detail.

From the Editors

Materials and Methods

Cell Lines, Expression Vectors, and Transfections

Three ER-positive, noninvasive, and nonmetastatic human breast cancer cell lines, MCF-7, T47D, and ZR75.1 (28) (ATCC, Manassas, VA), were maintained in Dulbecco's minimal essential medium supplemented with 10% fetal bovine serum, 100 U/mL penicillin, and 100 μg/mL streptomycin (Invitrogen, Carlsbad, CA). To prepare serum-free conditioned medium (CM), 2×10^7 cells per flask of each cell type were washed three times and incubated for 24 hours at 37°C with 15 mL serum-free culture medium. The medium was harvested, centrifuged at 1250 *g* for 5 minutes at 4°C, and passed through a 0.22-μm filter. CM was 30× concentrated at 4°C in Centriprep tubes YM-10 (Millipore, Billerica, MA).

To generate cells that expressed green fluorescent protein (GFP)–Rab fusion proteins, *Rab3D*, *Rab27A*, and *Rab27B* cDNAs were fused in-frame to GFP into the peGFP-C1 vector (Clontech, Mountain View, CA) and confirmed by sequencing. The source of *Rab27B* and *Rab27A* cDNA and GFP fusion constructs were described previously (29,30); the *Rab3D* cDNA was purchased from Origene, Inc (Rockville, MD). Mutant forms of *Rab27B* that encoded the T23N, N133I, and Q78L proteins and a geranylgeranyl-binding mutant (GER) were generated by polymerase chain reaction (PCR) site-directed mutagenesis (Retrogen, Inc, San Diego, CA). Breast cancer cell lines MCF-7, T47D, and ZR75.1 that stably or transiently overexpressed GFP-Rab fusion proteins were then generated by electroporation using the Cell Line Nucleofector Kit V according to the manufacturer's protocol (Amaxa, Gaithersburg, MD). To establish stable cell lines, transfected cells were selected in G418 (1 mg/mL) (Invitrogen) for 4 weeks. At least four clones of each cell line were used for in vitro experiments to exclude clonal variation. Animal experiments were performed with one representative clone except for wild-type (WT) GFP-Rab27B cells, of which four clones were tested.

Rab27B-specific HiPerformance-guaranteed small interfering RNAs (siRNAs) (siRab27B-1 target = 5′ AAA CGT GTG GTT TAT AAT GCA 3′ and siRab27B-2 target = 5′ TAG GAA TAG ACT TTC GGG AAA 3′) and a scrambled RNA interference (RNAi) negative control were purchased from Qiagen (Venlo, the Netherlands). RNAi transfections were performed by electroporation using the Cell Line Nucleofector Kit V according to the manufacturer's protocol (Amaxa).

Antibodies and Reagents

The following primary antibodies were used for western blot analysis or immunohistochemistry (IHC): mouse monoclonal anti-GFP (1:1000) (MAB3580; Millipore), mouse monoclonal anti-tubulin (1:1000) (T5168; Sigma–Aldrich, St Louis, MO), rabbit polyclonal anti-Rab27B (1:1000) (31), mouse monoclonal anti-cyclin E (1:500) (AHF0312; Invitrogen), mouse monoclonal anti-cyclin A (1:250) (33-4900; Zymed Laboratories, San Francisco, CA), rabbit monoclonal anti-Ki67 (1:25) (RM-9106-R7; NeoMarker, Fremont, CA), rabbit polyclonal anti-p27 (1:1000) (sc-527; Santa Cruz Biotechnology, Santa Cruz, CA), rabbit polyclonal anti–heat-shock protein (HSP)90α and HSP90β (1:1000) (PA3-012, PA3-013; Affinity Bioreagents, Golden, CO). Secondary antibodies coupled to horseradish peroxidase, Alexa-444, Alexa-555, or biotin were obtained from Amersham Pharmacia Biotech (Diegem, Belgium) or Invitrogen. The nuclear stain, 4′,6-diamidino-2-phenylindole (DAPI), and a filamentous actin stain, phalloidin–tetramethyl rhodamine isothiocyanate, were purchased from Sigma–Aldrich.

The HSP90 inhibitors, geldanamycin and 17-(allylamino)-17-demethoxygeldanamycin (17-AAG) were purchased from Biomol (Exeter, UK). A rabbit polyclonal anti-HSP90α neutralizing antibody (SPS-771) and the HSP90α and HSP90β recombinant

proteins were obtained from Stressgen (Ann Arbor, MI). Recombinant pro-matrix metalloproteinase (MMP)-2 protein and the human Proteome Profiler apoptosis antibody array were obtained from R&D systems (Minneapolis, MN). The apoptosis array allows the simultaneous detection of 35 apoptosis and proliferation-related proteins in a single sample and was used according to the manufacturer's protocol.

Invasion Assays

For the type I collagen invasion assay, the following precooled components were gently combined and defined as type I collagen solution: four volumes of type I collagen (stock is 3.49 mg/mL), five volumes of calcium- and magnesium-free Hank balanced salt solution, one volume of MEM (10×), one volume of 0.25 M NaHCO3, 2.65 volumes of culture medium, and 0.3 volumes of 1 M NaOH. For each test condition, 1.25 mL of type I collagen solution was added to one well of six-well plate, homogeneously spread and gelified on a flat surface in a humidified atmosphere of 10% CO2 in air at 37°C for at least 1 hour. GFP- or Rab-transfected MCF-7, T47D, or ZR75.1 single cells (2×10^5) suspended in 1 mL culture medium were seeded on top of the type I collagen gel and incubated on a flat surface in a humidified atmosphere of 10% CO2 in air at 37°C. Test products such as geldanamycin, 17-AAG, anti-HSP90α neutralizing antibody, and HSP90 recombinant proteins were added to the culture medium in the desired concentrations.

Cell morphology was studied, and invasion was scored after 24 hours (32). The factor shape refers to a value that is affected by an object's shape but is independent of its dimensions. It was calculated as $(\text{perimeter})^2/(4\pi \text{ area})$, which describes the deviation of an object from a geometric circle. It gives a minimal value of 1 for a perfect circle and larger values for shapes having a higher ratio of perimeter to area. The number of invasive and noninvasive cells was counted in 10 randomly selected microscopic fields with a 20× objective and 10× eye piece by two blinded observers using an inverted phase-contrast microscope (DMI 3000B; Leica, Wetzlar, Germany). The invasion index was calculated as the ratio of the number of cells that invaded the gel divided by the total number of cells counted in each field. Collagen matrices were fixed in 3% paraformaldehyde for 10 minutes and phalloidin–tetramethyl rhodamine isothiocyanate stained as previously described (32). Cells were imaged with a Zeiss 510 META confocal laser scanning microscope (Carl Zeiss, Micro-imaging, Inc, Heidelberg, Germany) using a 488 argon and a 543 helium–neon laser. Images were acquired using a Plan Apochromat 63× Phase 1.4 oil differential interference contrast objective or a Plan Apochromat 100× Phase 1.4 oil differential interference contrast objective. All of the images shown are collapsed z-stacks.

For the Matrigel invasion assays, 10^5 cells in serum-free culture medium were plated in the top transwell chamber with Matrigel-coated membrane (24-well insert; pore size 8 μm; Becton Dickinson, Franklin Lakes, NJ); culture medium was used as a chemoattractant in the lower chamber (33). After 48 hours, a cotton swab removed the cells that did not invade through the pores. Cells on the lower surface of the membrane were stained with DAPI. Invasive cells were counted in 10 microscopic fields per filter using a fluorescence microscope (Axiovert 200M; Carl Zeiss) with a 40× objective.

Protein Analysis

For western blot analysis, MCF-7 cells ($1–10 \times 10^6$) were harvested in Laemmli lysis buffer (0.125 M Tris–HCl [pH 6.8], 10% glycerol, 2.3% sodium dodecyl sulfate [SDS]). Cell lysates (25 μg) and CM (20 μL) were suspended in 10 μL reducing sample buffer (1 M Tris–HCl [pH 6.8], 30% glycerol, 6% SDS, 3% β-mercaptoethanol, 0.005% bromophenol blue) and boiled for 5 minutes at 95°C. Samples were run on NuPAGE 4%–20% Bis–Tris gradient gels (Invitrogen), transferred to polyvinylidene fluoride membranes, blocked in 5% nonfat milk in phosphate-buffered saline (PBS) with 0.5% Tween-20, and immunostained. Scanning densitometry was carried out with the Quantity One Program (Bio-Rad, Hercules, CA).

Quantitative determination of HSP90α in medium that was conditioned by MCF-7 breast cancer cells stably expressing GFP and GFP-Rab27B was performed with a HSP90α enzyme-linked immunosorbent assay kit (Stressgen) according to the manufacturer's instructions.

For gelatin zymography, CM (20 μL) was resuspended in 10 μL nonreducing sample buffer (0.5 M Tris–HCl [pH 6.8], 20% glycerol, 4% SDS, 0.005% bromophenol blue) without boiling. Samples were loaded on Novex 10% zymogram gelatin substrate gels (Invitrogen). After electrophoresis, gels were washed twice for 30 minutes in a 2% Triton X-100 (Bio-Rad) water solution at room temperature and incubated overnight at 37°C in MMP substrate buffer (50 mM Tris–HCl [pH 7.5], 10 mM $CaCl_2$). Gels were rinsed again in distilled water and stained with Coomassie Brilliant Blue as described above. Proteolytic activities appeared as clear bands of lysis against a dark background of stained gelatin.

Flow Cytometric Cell Cycle Analysis and Cell Proliferation Assay

For analysis of cell cycle distribution, the Coulter DNA Prep Reagents Kit (Beckman Coulter, Fullerton, CA) was used. Serum-induced cell cycle progression was analyzed by growing MCF-7 GFP and GFP-Rab27B stably transfected cells to 50% confluence, followed by serum starvation for 24 hours, and incubation in Dulbecco's minimal essential medium supplemented with 0.5% fetal bovine serum, 100 U/mL penicillin, and 100 μg/mL streptomycin (Invitrogen) for 24 hours. Cells were harvested by trypsinization, washed with PBS and exposed to DNA Prep Lyse for 1 minute, followed by incubation with DNA Prep Stain for 15 minutes at room temperature in the dark. Cellular DNA content was monitored on a Beckman Coulter Cytomics FC500 flow cytometer (Beckman Coulter). Cell cycle fractions were quantified using WinCycle software (Phoenix Flow Systems, San Diego, CA).

To examine whether Rab27B affects cell proliferation in a GTP-, geranylgeranyl-, and HSP90α-dependent manner, three sets of experiments were conducted: 1) proliferation rates of MCF-7 cells stably expressing GFP, GFP-Rab27B, GFP-Rab27B-Q78L, GFP-Rab27B-T23N, and GFP-Rab27B-GER were compared; 2) proliferation rates of MCF-7 GFP-Rab27B cells transiently targeted with control or Rab27B siRNAs were studied; and 3) proliferation rates of MCF-7 GFP cells, treated with recombinant HSP90α, and MCF-7 GFP-Rab27B cells, challenged with control IgG or anti-HSP90α neutralizing antibody, were evaluated. To obtain a growth curve under each condition, triplicate wells of seeded cells were each counted five times. Two investigators independently counted the

total number of cells in each well every 2 days for a total of 8 days with the use of a manual hemocytometer.

Animal Studies

Animal studies were in accordance with a protocol approved by the Local Ethics Committee of Ghent University Hospital. At the age of 4 weeks (1 week before cell inoculation), female Swiss nu/nu mice (10 mice per group) (Charles River Laboratories, Brussels, Belgium) were primed with a 1 mg estradiol pellet (Organon Laboratories, Cambridge, UK) implanted subcutaneously in the neck through surgical incision. Viable cells were injected into the mammary fat pad as a 50 μL suspension of 10^6 cells in Matrigel (Becton Dickinson). Tumor volume was estimated by using the equation, $V = 0.4 \times a \times b^2$, where V is volume, a is the length of the major axis of the tumor, and b is the length of its minor axis. Intraperitoneal metastasis formation was assessed weekly via palpation and visual analysis of the blue and swollen appearance of the abdomen. Mouse survival time was defined as the time from injection until the animals died or were euthanized by cervical dislocation per the protocol approved by the ethics committee, which specifically limited hemorrhagic ascites formation.

Development of ascites was monitored by the measurement of abdominal circumference and body weight. Ascites formation was scored positive when the abdominal circumference increased at least 15%. For the assessment of survival, per Local Ethics Committee of Ghent University Hospital guidelines, mice were euthanized when the abdominal circumference increased 60% above normal controls. Ascites fluid was collected, and hematological parameters (number of erythrocytes, hemoglobin, and hematocrit) were evaluated by flow cytometry using an ADVIA 120 Hematology System (Bayer Corporation, Tarrytown, NY).

Primary tumors and peritoneal metastasis were extracted, weighed, and fixed in 4% buffered formol for 12 hours, followed by a wash with PBS and transfer to 70% ethanol, and then embedded in paraffin, sectioned, and stained with hematoxylin and eosin. Lung, liver, and spleen were analyzed for macroscopic metastasis. IHC using anti-Rab27B and anti-Ki67 antibodies was performed on paraffin sections, using an NexES automated slide staining system (Ventana Medical Systems, Tucson, AZ). Primary tumors were scored as invasive if they were firmly attached to the abdominal wall and if hematoxylin and eosin staining revealed massive infiltration of the muscular tissue of the abdominal wall by cancer cells. Proliferation was quantified as the percentage of Ki67-positive cancer cells per high-power field (objective 40× and eye piece 10×) averaged across 18 images from a total of three primary tumors per cell line.

GFP-Rab27B Vesicle Isolation

Parental or GFP-Rab27B MCF-7 cells (2×10^8 cells) were trypsinized and resuspended in culture medium. The cell suspension was centrifuged for 10 minutes at 500*g*, followed by three washes with 5 mL Dulbecco's PBS (PBS^{D+}). The cell pellet was resuspended in 1 mL homogenization solution (250 mM sucrose in PBS^{D+} supplemented with protease inhibitor cocktail [Roche Applied Science, Indianapolis, IN]). Cells were homogenized on ice via sonication on a Vibracell VCX130 (4 pulses of 5 seconds with amplitude of 30% each separated by 15-second intervals) (Sonics and Materials, Inc, Newton, CT). Different centrifugations were performed using a 70.1 Ti rotor Beckman Coulter centrifuge (Beckman Coulter): low-speed centrifugation at 3000*g* for 10 minutes at 4°C, followed by high-speed centrifugation at 30 000*g* for 60 minutes at 4°C. A sample of the supernatant and the pellet was collected after each centrifugation step to confirm the presence of vesicle membrane–bound GFP-Rab27B in the supernatant via western blot analysis. Next, the supernatant was incubated at a 1:1 ratio (vol/vol), with anti-GFP–labeled magnetic microbeads suspended in homogenization solution (50 μL microbeads/10×10^6 cells) (MACS MicroBeads; Miltenyi Biotec, Auburn, CA) for 30 minutes on ice. Total samples (2 mL) were loaded on the automated MACS separator (Miltenyi Biotec). Vesicles were eluted in elution buffer (Miltenyi Biotec). After elution, homogenization buffer was added in a 1:1 (vol/vol) ratio. The purity of the vesicle fraction was checked before and after magnetic separation via flow cytometry (Calibur; Becton Dickinson). Vesicles were pelleted by centrifugation at 140 000*g* for 1 hour.

Liquid Chromatography–Mass Spectrometry/Mass Spectrometry

Vesicle pellets and CM (20 μL) were suspended in 60 and 10 μL reducing sample buffer, respectively (1 M Tris–HCl [pH 6.8], 30% glycerol, 6% SDS, 3% β-mercaptoethanol, 0.005% bromophenol blue) and boiled for 5 minutes at 95°C. Samples were run on NuPAGE 4%–20% Bis–Tris gradient gels (Invitrogen) in denaturating SDS buffer, stained with 0.5% Coomassie Brilliant Blue (Bio-Rad) in 40% methanol and 10% acetic acid for 20 minutes, and destained in a solution composed of 40% methanol and 10% acetic acid. Gel bands were processed and analyzed by liquid chromatography–mass spectrometry/mass spectrometry (LC-MS/MS) as previously described (34). Raw MS/MS files were submitted to the NIH MASCOT Cluster (35) using MASCOT DAEMON. Data were searched against the UNIPROT-SPROT + UNIPROT-TREMBL database as described (34). For each peptide identification, MASCOT reports a probability-based ion score, which is defined as $-10 \times \log10(P)$, where P is the absolute probability that the observed match between the experimental data and the database sequence is a random event. The significance threshold for inclusion of each peptide in the output file is the individual ion score meeting or exceeding its MASCOT identity score threshold ($P < .05$). MASS SIEVE was used to parse the MS/MS data from MASCOT and generate protein parsimony reports (http://www.proteomecommons.org/dev/masssieve). Each protein was assigned to the functional classification based on the Gene Ontology annotation system using the DAVID database bioinformatics resources (http://david.abcc.ncifcrf.gov) (36). Only peptides that were detected in two separate experiments were retained.

Patient Samples, Quantitative Real-Time PCR, IHC, and Fluorescence In Situ Hybridization

Clinical data and primary breast carcinoma samples were collected for every consecutive patient with stages I–IV breast cancer at Ghent University Hospital between January 11, 2008, and December 31, 2008. Written informed consent was obtained from each patient according to the recommendations of the local ethics

committee. Adjacent histologically normal breast tissue was collected in the same tissue sample from each patient. One part of the tumor, with adjacent normal tissue, was snap-frozen immediately and stored at −80°C for blinded quantitative real-time PCR and western blot analysis and one part containing tumor and normal cells was formalin-fixed for Rab27B IHC.

Western blotting was performed on lysates prepared from microdissected tumor tissue. Briefly, one section stained with hematoxylin and eosin was mounted with a coverslip, and the remaining adjacent serial sections were left without a coverslip for tissue removal. Using the covered slide stained with hematoxylin and eosin as the template, areas that were not of interest (containing stroma and accumulated collagen) were removed. The remaining epithelial tissue, obtained from a minimum of 10 sections, was lysed and analyzed by western blotting.

The Rab27B protein IHC signal was scored on the following scale taking into account both the proportion of cells stained and the intensity staining in those cells: score 0, weak or absent cytoplasmic staining and less than 5% of cancer cells containing Rab27B localized to the plasma membrane or vesicle clusters; score 1, cytoplasmic staining and between 5% and 30% of the cancer cells containing Rab27B localized prominently to the plasma membrane or clustered vesicles; score 2, cytoplasmic staining and more than 30% of the cancer cells containing Rab27B localized prominently to the membrane and vesicles; two observers quantified independently.

Total RNA was isolated using the Trizol reagent (Invitrogen) according to the manufacturer's protocol. RNA was treated with a DNase kit (DNA-free) to remove all remaining DNA according to the manufacturer's protocol (Applied Biosystems, Austin, TX). RNA concentration and purity were measured on the Nanodrop ND-1000 (Nanodrop Technologies, Wilmington, DE). First-strand cDNA was synthesized using a high-capacity RNA-to-cDNA kit (Applied Biosystems) according to the manufacturer's guidelines. Quantitative real-time PCR was performed using 100 ng cDNA, Taqman gene expression master mix reagent, and Assays-On-Demand (Applied Biosystems) for *Rab27B* (Assay ID Hs00188156_m1), *Rab27A* (Assay ID Hs00608302_m1), *Rab3D* (Assay ID Hs00269915), and a control gene, *PIAA* (37) (Assay ID Hs99999904_m1), on an ABI PRISM 7900 HT Sequence Detection System (Applied Biosystems) using the comparative C_T method ($\Delta\Delta C_T$), an approach to measure relative gene expression. The cycling conditions were as follows: 2 minutes at 50°C, 10 minutes at 95°C, and 40 cycles at 95°C for 15 seconds and 60°C for 60 seconds.

Fluorescence in situ hybridization was performed with a dedicated *Rab27B* probe set (RP11-99A1 and RP11-839G9; Chori, BACPAC Resources, Oakland, CA). Deparaffinized and heat-pretreated tissue sections were digested with pepsin (in 8.5 mM NaCl [pH 2]; Sigma-Aldrich) and dehydrated in graded ethanol (75%, 80%, and 100%). The tissues on the slides were denatured at 82°C for 5 minutes and hybridized at 45°C for 18 hours with the *Rab27B* probe set in a S2450 Hybridizer Instrument for In Situ Hybridization (DAKO, Stockholm, Sweden). In each case, 20 nonoverlapping, intact, interphase tumor nuclei identified by DAPI staining were evaluated, and Rab27B copy numbers in each nucleus were assessed. The patient samples were considered to contain amplified, or polysomic *Rab27B* gene expression if more than two signals were seen in at least 10% of the tumor cells.

Statistical Analysis

All statistical calculations were performed using MedCalc (Version 11.0; MedCalc Software, Mariakerke, Belgium). Comparisons were performed using a two-sided unpaired Student *t* test following D'Agostino–Pearson testing for normal distribution (Matrigel invasion assays, factor shape calculation, Ki67 proliferation index, and tumor weight) or χ^2 test (collagen type I invasion assays). For the cell proliferation assays, data were compared by two-way repeated measures analysis of variance test. Kaplan–Meier curves and log-rank testing were used for survival analyses. *Rab27B*, *Rab27A*, and *Rab3D* mRNA levels in clinical samples were compared with the Mann–Whitney rank sum test. Frequency tables of the Rab27B IHC data were analyzed by the χ^2 test. All data presented are representative of at least three independent experiments. All statistical tests were two-sided. *P* values less than .05 were considered to be statistically significant, and where appropriate, the difference of means and the 95% confidence interval (95% CI) are indicated.

Results

Effect of Rab27B Overexpression on Morphology and Invasion

After transient transfection of human MCF-7 breast cancer cells, GFP-tagged Rab3D, Rab27A, and Rab27B each displayed a vesicular distribution (Figure 1, A). MCF-7 cells transfected with a GFP control plasmid exhibited no morphological changes, whereas those transfected with GFP-Rab3D or GFP-Rab27A exhibited limited ruffling at the cell surface (Figure 1, A). By contrast, cells in which GFP-Rab27B was overexpressed formed cellular extensions and a spread morphology and had a statistically significantly increased ability to invade Matrigel compared with the other three transfected cell types (number of invading cells, Rab27B expressing vs control, mean = 60.1 vs 5.0 cells, difference = 55.1 cells, 95% CI = 49.6 to 60.6 cells; $P < .001$) (Figure 1, B). When MCF-7, T47D, or ZR75.1 breast cancer cells were transfected with GFP-Rab27B, the cells assumed a similarly changed morphology and were more invasive than control cells on a type I collagen substrate (number of invading cells of the total number of cells, Rab27B expressing vs control: MCF-7 cells, 24 of 234 [10%] vs two of 212 [0.9%], $P < .001$; T47D cells, 16 of 229 [7%] vs five of 215 [2%], $P = .02$). GFP-Rab27A and GFP-Rab3D had no such effect (Figure 1, C and D, and data not shown).

Involvement of Rab27B in Matrix Invasion and G_1 to S Phase Cell Cycle Progression

Next, we established MCF-7 cells that stably expressed GFP, GFP-Rab27B, GFP-Rab27A, and each of four mutants of GFP-Rab27B; GFP-Rab27B-Q78L is a constitutively active mutant defective in GTP hydrolysis, GFP-Rab27B-T23N and GFP-Rab27B-N133I are dominant negative mutants defective in GTP binding, and the GFP-Rab27B-GER mutant is impaired in geranylgeranyl modification and vesicle membrane targeting (Supplementary Figure 1, available online).

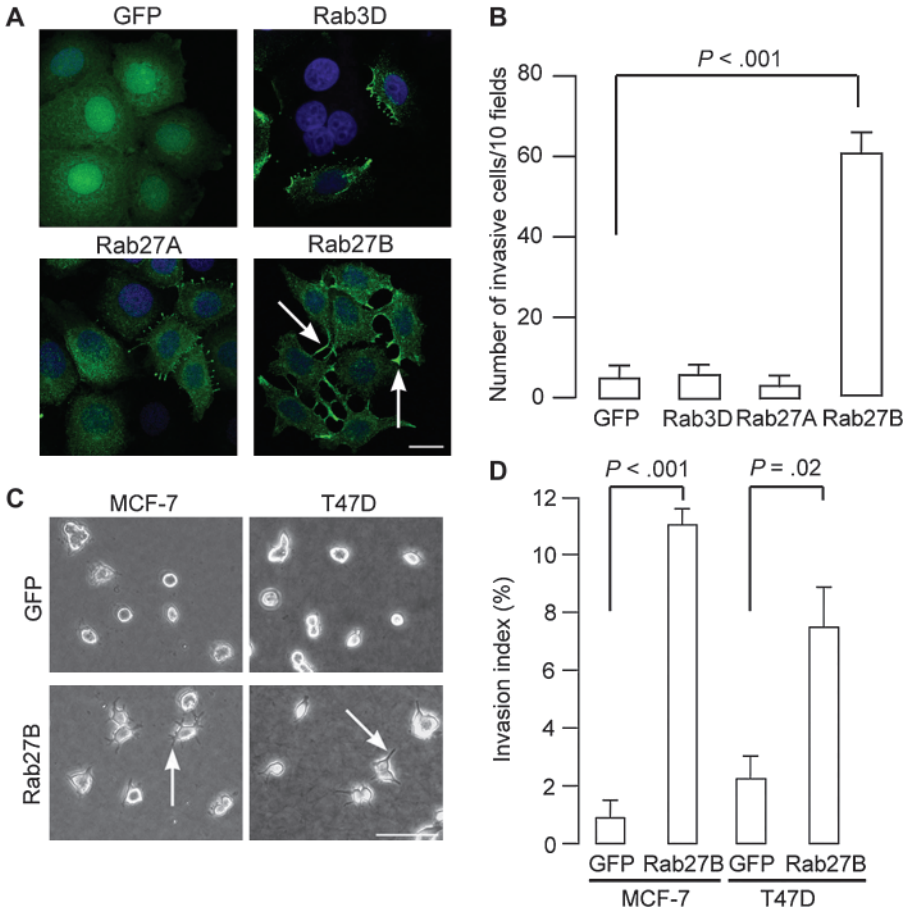

Figure 1. Effect of ectopic expression of Rab3D, Rab27A, or Rab27B on the formation of cellular extensions and invasiveness. **A**) Morphology of MCF-7 cells transiently transfected with green fluorescent protein (GFP), GFP-Rab3D, GFP-Rab27A, or GFP-Rab27B-expressing plasmids. Twenty-four hours after transfection, cells were fixed and nuclei were stained with 4′,6-diamidino-2-phenylindole (DAPI) (**blue**). Laser scanning confocal images show punctuate GFP signal (**green**) that is indicative of localization of GFP fusion protein to vesicles. Scale bar, 20 μm. **B**) Matrigel invasion assay with GFP-Rab–transfected MCF-7 cells. Twenty-four hours after transient transfection with GFP-Rab–expressing plasmids, 10^5 MCF-7 cells were seeded on top of a Matrigel-coated filter, and their migration toward medium containing serum was quantified by microscopic evaluation (total magnification ×400). The mean total number of invading cells counted after 72 hours from 10 different fields is shown with the upper 95% confidence intervals from the means of three independent experiments performed in triplicate. *P* values were calculated using two-sided Student *t* tests. Statistically significant *P* values are indicated. **C** and **D**) Morphology and invasiveness of GFP-Rab–transfected MCF-7 and T47D breast cancer cells. In (**C**), phase-contrast images are shown of cells seeded on type I collagen matrix 24 hours after transient transfection. In **(D),** the invasion index was calculated by counting the number of invading and noninvading cells into type I collagen matrix in 10 fields. Invasion indices are means and upper 95% confidence intervals derived from the means of three independent experiments performed in triplicate. *P* values were calculated using χ^2 tests; statistically significant *P* values are indicated. Scale bar, 50 μm. In (**A**) and (**C**), **arrows** indicate cellular extensions and local spreading.

Laser scanning confocal microscopy revealed a vesicular distribution for the GFP-Rab27A, GFP-Rab27B, and GFP-Rab27B-Q78L proteins in these cells but a complete loss of vesicular localization for the GFP-Rab27B-T23N and GFP -Rab27B-GER proteins (Supplementary Figure 2, available online). Local spreading and invasion in type I collagen, apparent in GFP-Rab27B–transfected breast cancer cells, were also characteristic of GFP-Rab27B-Q78L–transfected cells (number of invading cells of the total number of cells, WT GFP-Rab27B–expressing cells vs GFP-Rab27B-Q78L–expressing cells vs control: 27 of 224 [12%] vs 27 of 210 [13%] vs 3 of 211 [1%]; $P < .001$, for both GFP-Rab27B WT and Q78L vs control) (Figure 2, A and B). By contrast, GFP-Rab27A, GFP-Rab27B-T23N, GFP-Rab27B-N133I, and GFP-Rab27B-GER–expressing MCF-7 cells did not change morphology nor invade the collagen matrix. F-actin staining with phalloidin–tetramethyl rhodamine isothiocyanate revealed a rounded appearance for MCF-7 GFP control cells, with membrane blebs and prominent cortical F-actin (Figure 2, C). MCF-7 GFP-Rab27B cells showed elongated cell morphology, with multiple protrusions. GFP-Rab27B vesicles accumulated at the cell periphery (Figure 2, C). We quantified cell spreading by calculating the factor shape of the cells, $(\text{perimeter})^2/(4\pi \text{ area})$, which describes the deviation of the shape from a geometric circle. For control cells, this value was 1.65 ± 0.23, indicating poor spreading; for GFP-Rab27B cells, the value was 5.59 ± 0.35, indicating statistically significant spreading (difference = 3.94, 95% CI = 3.74 to 4.13, $P < .001$). Transient targeting of Rab27B by single or pooled siRNAs depleted Rab27B protein by 70%–80%, as assessed by western blotting, and was accompanied by loss of the elongated cell morphology (factor shape value, after transfection with pooled siRNAs, was 2.1 ± 0.3) and loss of invasion into Matrigel and collagen type I matrices (Figure 2, D, and data not shown).

Next, we investigated the impact of Rab27B expression on cell cycle progression and proliferation. The results of a screen using a commercial "proteome profiler" antibody array indicated that ectopic expression of GFP-Rab27B was associated with a mitogenic signature in MCF-7 cells (data not shown). Cell cycle progression was studied by flow cytometric cell cycle analysis after serum starvation followed by readdition of 0.5% serum. We found that GFP-Rab27B initiates G_1 to S phase transitions in MCF-7 cells (Figure 2, E). In addition, expression of the positive cell cycle regulators cyclin A and cyclin E increased, whereas expression of the negative cell cycle regulator p27 decreased, in MCF-7 cells transfected with GFP-Rab27B or GFP-Rab27B-Q78L (Figure 2, F). By contrast, transfection of GFP-Rab27B-T23N, -N133I, or -GER was associated with increased expression of p27 but reduced expression of cyclin A and cyclin E. MCF-7 cells that expressed GFP-Rab27B consistently demonstrated much higher levels of cell proliferation than control cells transfected with only GFP at limiting (0.5%) serum concentrations ($P < .001$) (Figure 2, G). Furthermore, GFP-Rab27B enhanced MCF-7 proliferation under

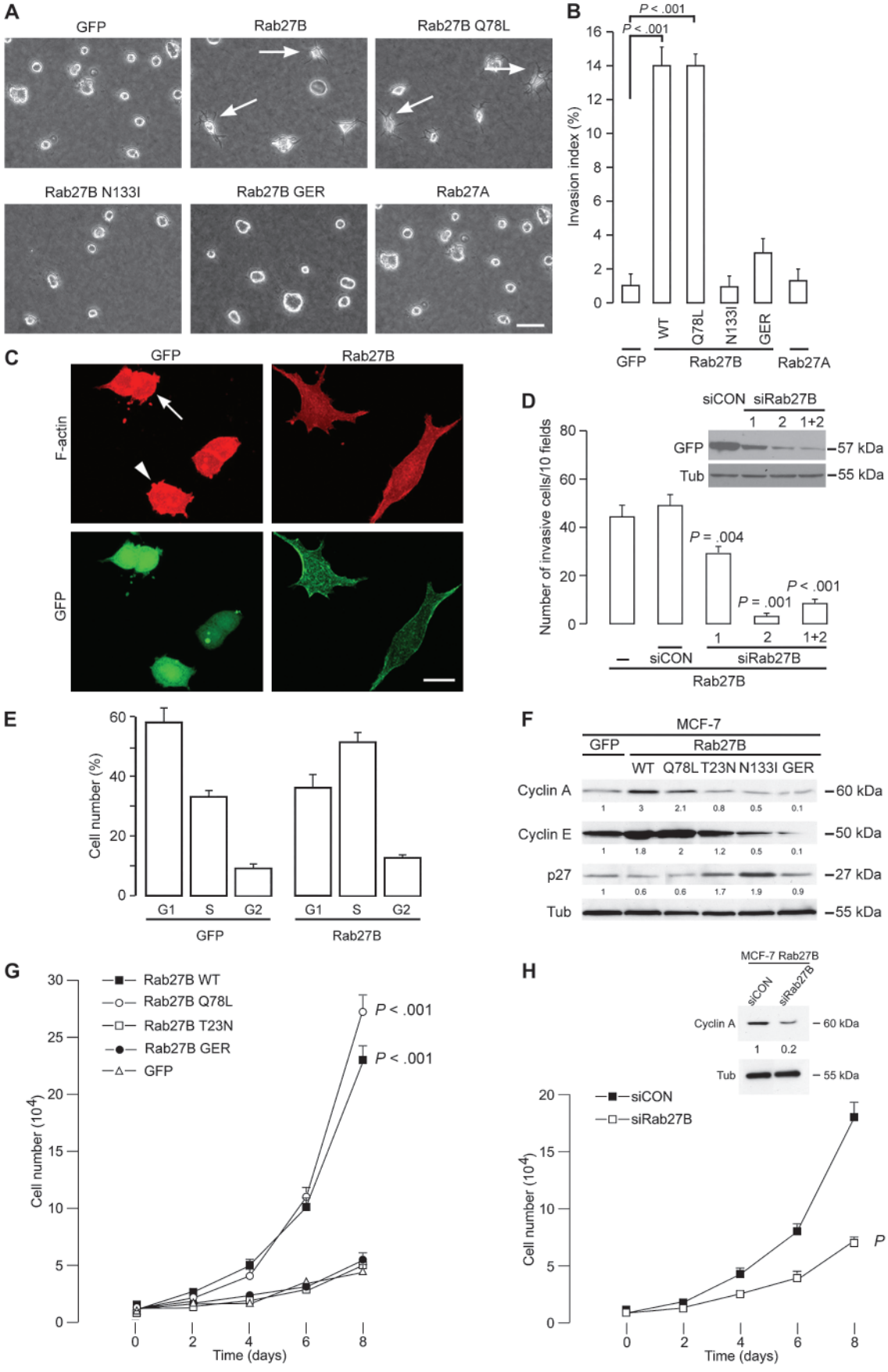

(continued)

limiting serum concentrations in a GTP- and geranylgeranyl-dependent manner. A similar enhancement of growth under low serum concentrations was observed following transfection of GFP-Rab27B into T47D and ZR75.1 breast cancer cells (data not shown). In supporting experiments, transient targeting of Rab27B by a combination of both siRNAs precluded Rab27B-stimulated proliferation ($P < .001$) and Rab27B-induced cyclin A expression (Figure 2, H).

Effect of Rab27B Overexpression on Invasive Tumor Growth in Nude Mice

To further investigate whether Rab27B enhances invasive tumor growth in vivo, we implanted 10^6 MCF-7 cells stably transfected with GFP-Rab27A, or GFP-Rab27B and its mutants, or a similar number of control GFP-transfected MCF-7 cells into the mammary fat pads of Swiss nu/nu mice and monitored tumor and metastasis formation for 10 weeks. All mice displayed visible mammary tumors 2 weeks after injection. No apparent toxicity was observed in mice bearing control MCF-7 GFP xenografts (n = 10), but 37.5% of the mice bearing MCF-7 GFP-Rab27B xenografts (n = 40) developed hemorrhagic ascites in the peritoneal cavity that resulted in death (at 10 weeks, MCF-7 GFP- vs GFP-Rab27B–injected mice, survival was 100% vs 62.5%, hazard ratio of death = 0.26, 95% CI = 0.08 to 0.88, $P = .03$) (Figure 3, A and B). Ascites fluid was collected from six of these mice; the mean volume was 1.6 ± 0.2 mL, and the number of red blood cells present was approximately 20% of that in the peripheral blood ($2.2 \pm 0.35 \times 10^6/mm^3$). The tumor aggregates present in the ascites yielded a 57-kDa GFP-Rab27B immunoreactive protein (Figure 3, C), indicating they were derived from the xenograft, and consisted of a rim of five to 10 cell layers surrounding a necrotic center (Figure 3, D).

The primary MCF-7 GFP-Rab27B xenografts showed massive muscular invasion compared with the MCF-7 GFP xenografts (Figure 3, E). At 10 weeks, approximately 80% and 60% of nude mice injected with GFP-Rab27B and GFP-Rab27B-Q78L MCF-7 cells, respectively, developed invasive xenografts (Figure 3, F). By contrast, MCF-7 xenografts that expressed GFP alone, GFP-Rab27B-T23N, GFP-Rab27B-N133I, GFP-Rab27B-GER or GFP-Rab27A were nearly all noninvasive, that is, confined within fibrotic capsules. IHC of the primary GFP-Rab27B xenograft with a specific Rab27B antibody (Supplementary Figure 3, available online) revealed Rab27B localization in the cytoplasm and at cell–cell contacts (Figure 3, G). Also at 10 weeks, the MCF-7 GFP-Rab27B and GFP-Rab27B-Q78L xenografts had an approximately eightfold larger volume and fourfold increased resected tumor weight than the MCF-7 GFP, GFP-Rab27B-T23N, GFP-Rab27B-N133I, GFP-Rab27B-GER, and GFP-Rab27A xenografts (means: weight of control GFP xenograft = 0.11 g, WT xenograft = 0.39 g, Q78L xenograft = 0.35 g; difference: control vs WT= 0.28 g, 95% CI = 0.26 to 0.30, $P < .001$; difference, control vs Q78L = 0.24 g, 95% CI = 0.21 to 0.26, $P < .001$) (Figure 3, H and I). Furthermore, Ki67 staining showed that 86% of MCF-7 GFP-Rab27B cancer cells were in a proliferative state compared with 33% of MCF-7 GFP cells (difference = 53%, 95% CI = 48% to 58%, $P < .001$) (Figure 3, J).

Functional Implication of HSP90α Secretion in Rab27B-Overexpressing Cells

GFP-Rab27B secretory vesicles were isolated from MCF-7 GFP-Rab27B cells by a combination of differential centrifugation and enrichment using anti-GFP antibody–coated magnetic beads and a benchtop automated magnetic cell sorter. Proteomic analysis was performed on 97% pure GFP-Rab27B vesicles, as measured by flow cytometry (Supplementary Figure 4, available online). The 1276 proteins that were identified with high confidence (ie, in two separate experiments) were assigned to 16 clusters that included proteins involved in vesicle trafficking, cellular metabolism, cell maintenance, cell signaling, GTPases, and chaperones (Supplementary Figure 4 and Supplementary Table 1, available online). HSP90α is known to play an essential extracellular role in cancer cell invasion (38) and was among the chaperones detected. Polyacrylamide gel analysis of the CM from MCF-7 GFP-Rab27B cells revealed 90 kDa proteins

Figure 2 (continued).

Figure 2. Rab27B GTP- and geranylgeranyl-dependent cancer cell invasion and cell cycle progression in vitro. **A**) Phase-contrast images showing morphology of MCF-7 cells stably transfected to express green fluorescent protein (GFP), GFP-Rab27A, GFP-Rab27B (wild type, WT), or GFP-Rab27B mutants. GFP-Rab27B-Q78L (constitutive active), -N133I (dominant negative), and -GER (impaired geranylgeranylation and vesicle targeting) were the mutants used. **Arrows** indicate cellular extensions and local spreading. Scale bar, 50 μm. **B**) Quantification of type I collagen invasion by the cells shown in (**A**). Invasion assays were performed as in Figure 1, D. Invasion indices are means and upper 95% confidence intervals derived from the means of three independent experiments performed in triplicate. *P* values were calculated using χ^2 tests. Statistically significant *P* values are indicated. **C**) Laser scanning confocal images of the F-actin cytoskeleton (phalloidin–tetramethyl rhodamine isothiocyanate) (**red**) and GFP (**green**) localization in MCF-7 GFP and GFP-Rab27B cells cultured for 24 hours on a collagen type I matrix. **Arrow** indicates cortical F-actin, and **arrowhead** indicates membrane blebs. Scale bar, 20 μm. **D**) Invasion by Rab27B-expressing MCF-7 cells in which Rab27B was depleted. MCF-7 cells that expressed GFP-Rab27B, with or without transfection of control small interfering RNA (siRNA) (siCON) or Rab27B siRNAs (siRab27B-1 and/or -2), were seeded on a Matrigel-coated filter. The inset panel shows the impact of the Rab27B siRNAs on Rab27B expression in these cells by immunoblotting. The numbers of invasive cells were counted after 72 hours in 10 different fields and are expressed as the mean with upper 95% confidence intervals of three independent experiments performed in triplicate. *P* values shown are for comparisons with the siCON transfection using two-sided Student *t* tests. **E**) Effect of Rab27B on cell cycle progression. MCF-7 GFP and GFP-Rab27B cells were grown to 50% confluence, followed by 24 hours serum starvation, and 24 hours serum-induced (0.5%) cell cycle progression. Percentages of MCF-7 GFP and GFP-Rab27B cells in G_1, S, and G_2 stage of the cell cycle, as measured by flow cytometry, are represented as the means with upper 95% confidence intervals of two independent experiments. **F**) Western blot analysis in mutant Rab27B-transfected MCF-7 cells of the positive (cyclin A and E) and negative (p27) G_1 to S phase cell cycle regulators. Protein levels were quantified as immunostaining intensity relative to tubulin. **G**) Measurement of cell proliferation rates of MCF-7 cells stably expressing GFP, GFP-Rab27B, or GFP-Rab27B mutants as in (**A**). A total of 10000 cells were plated into each well of a total of 15 wells on day 1 to establish one growth curve under each condition in triplicate. The total number of cells per well was manually counted every 2 days until day 8. Mean number of cells is plotted with upper 95% confidence intervals. *P* values were calculated using the two-way repeated measures analysis of variance test. Statistically significant *P* values are indicated; data were compared with the GFP control. **H**) Measurement of cell proliferation rates of MCF-7 GFP-Rab27B cells transiently transfected with control (siCON) or pooled Rab27B siRNAs (siRab27B-1 and -2). The experiment was performed as in (**G**). An inset panel shows the effect of this siRNA on cyclin A expression in MCF-7 GFP-Rab27B cells. Tubulin was used as loading control.

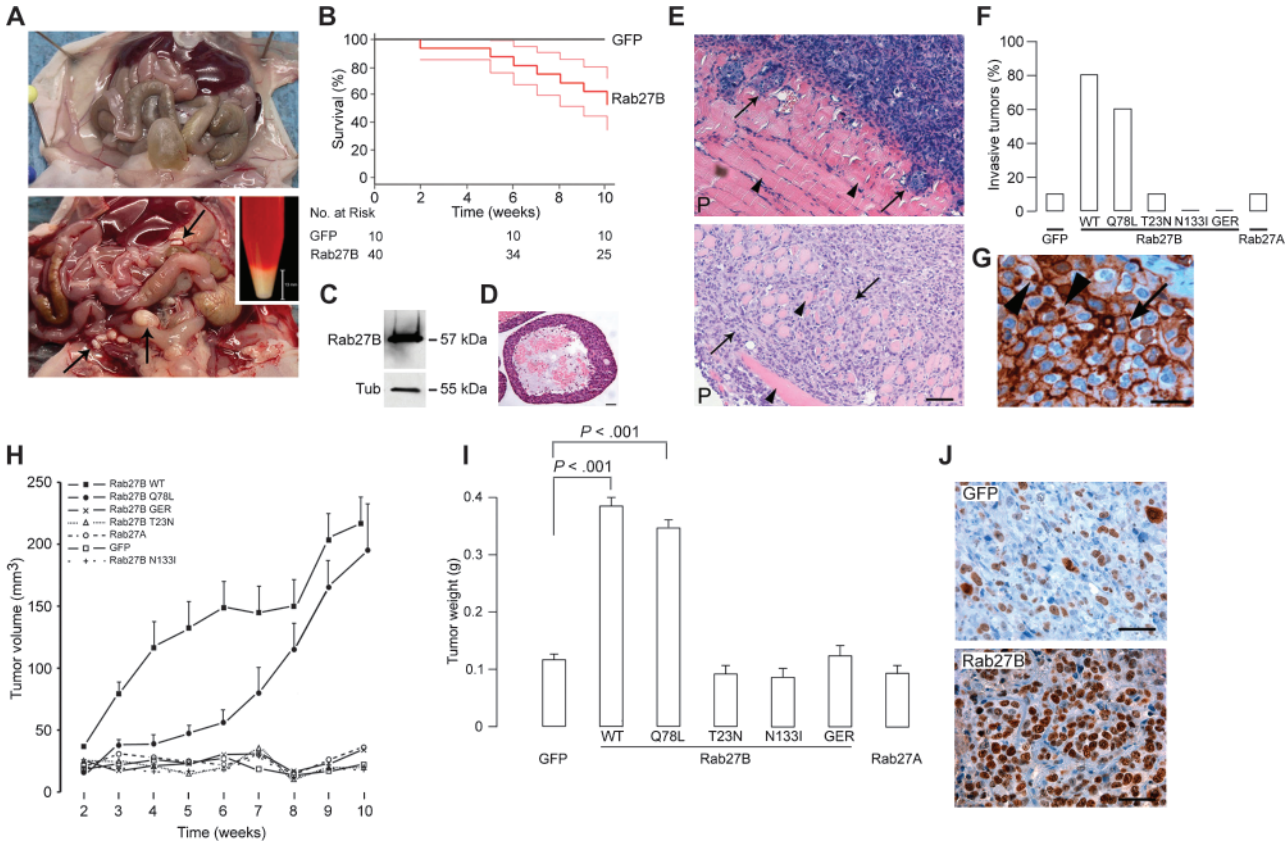

Figure 3. Effect of Rab27B on invasive tumor growth in vivo. Nude mice were injected in the mammary fat pad with MCF-7 cells expressing green fluorescent protein (GFP), GFP-Rab27A, GFP-Rab27B (wild type, WT), or mutant GFP-Rab27B proteins (Q78L, T23N, N133I, and GER). **A**) Tumorigenesis in nude mice with MCF-7 GFP-Rab27B xenografts vs controls. Mice with MCF-7 GFP-Rab27B xenografts (**lower panel**) developed hemorrhagic ascites (blue and swollen appearance of the ventral side) and tumor aggregates (**arrows**) in the peritoneal cavity and attached to organs such as the ovary. MCF-7 GFP xenografts (**upper panel**) developed no hemorrhagic ascites. **Inset**: Pelleted tumor aggregates from the peritoneal fluid of one mouse. Scale bar, 13 mm. **B**) Effect of Rab27B expression on survival of mice with xenografts. Kaplan–Meier curves with 95% confidence intervals and log-rank testing ($P = .031$) are shown for nude mice injected with MCF-7 GFP cells (n = 10) vs MCF-7 GFP-Rab27B cells (n = 40; four different clones with 10 mice per group). **C**) Expression of GFP-Rab27B in tumor aggregates. A western blot loaded with 60 μg peritoneal tumor aggregate and immunostained with primary Rab27B and tubulin antibodies is shown. **D**) Hematoxylin and eosin (H&E) staining of a peritoneal tumor aggregate. Scale bar, 100 μm. **E**) H&E staining of MCF-7 GFP (**upper panel**) and GFP-Rab27B (**lower panel**) xenografts. **Arrowheads** indicate striated muscle tissue; **arrows** indicate areas of muscular invasion by cancer cells to the peritoneal side (**P**). Scale bar, 100 μm. **F**) Relative invasiveness of xenografts expressing WT and mutant Rab27B proteins. Percentage of invasive tumors was determined by the total number of mice with an invasive xenograft in the peritoneal wall as assessed by macroscopic observation and immunohistochemistry (n = 10 mice per group). Precise percentages for a single experiment are shown. **G**) Cellular localization of Rab27B in MCF-7 GFP-Rab27B xenografts. **Arrow** indicates peripheral Rab27B distribution; **arrowheads** indicate Rab27B vesicle clustering appearing in the cytoplasm and at cell–cell contact. Scale bar, 25 μm. **H**) Mean tumor volume in nude mice bearing xenografts that expressed WT or mutant Rab27B proteins (n = 10 mice per group). Tumor size was assessed weekly by measurement of the external diameter of the xenografts for 10 weeks. GFP expression was maintained in the xenografts throughout this time period (data not shown). Error bars represent 95% confidence intervals. **I**) Mean tumor weight after surgical resection of xenografts expressing WT or mutant Rab27B proteins. Mice were killed at variable time points (ie, the ethical endpoint that limits hemorrhagic ascites formation or the experimental endpoint at 10 weeks) after injection of stably transfected MCF-7 cells (n = 10 mice per group). Error bars represent upper 95% confidence intervals. *P* values were calculated using two-sided Student *t* tests; statistically significant *P* values are indicated. **J**) Immunohistochemical staining of MCF-7 GFP and GFP-Rab27B xenografts to detect Ki67, a proliferation marker. The mean number of proliferating MCF-7 GFP-Rab27B cells, calculated from 18 images of three primary tumors per cell line, was 85.50 ± 4.04 vs 32.56 ± 2.68 proliferating control cells (two-sided Student *t* test, $P < .001$). Scale bar, 50 μm.

that were identified by mass spectrometry as HSP90α and HSP90β (Figure 4, A). Enzyme-linked immunosorbent assay assays confirmed that HSP90α secretion was sevenfold higher in the CM prepared from MCF-7 GFP-Rab27B cells compared with MCF-7 GFP cells (Figure 4, B). Western blotting measured HSP90α levels that were 4.4- and 4.9-fold higher in the CM of MCF-7 cells that expressed GFP-Rab27B and constitutively active GFP-Rab27B-Q78L, respectively, compared with CM from control MCF-7 GFP cells (Figure 4, C, upper panel); cells that expressed GFP-Rab27A, GFP-Rab27B-GER, or the GTP-binding mutant showed much less HSP90α secretion, that is, 0.4-, 0.4-, or 1.8-fold, respectively, that of MCF-7 GFP cells. However, western blot analysis revealed no difference in intracellular levels of HSP90α or HSP90β among MCF-7 cells expressing GFP, GFP-Rab27A, and GFP-Rab27B or its mutants (Figure 4, C, lower panel). In spite of this finding, 80% depletion of Rab27B protein expression by RNA interference (Figure 4, D, lower panel) was associated with a 50% reduction in HSP90α secretion into the CM of GFP-Rab27B MCF-7 cells (Figure 4, D, upper panel), whereas HSP90β secretion remained unchanged.

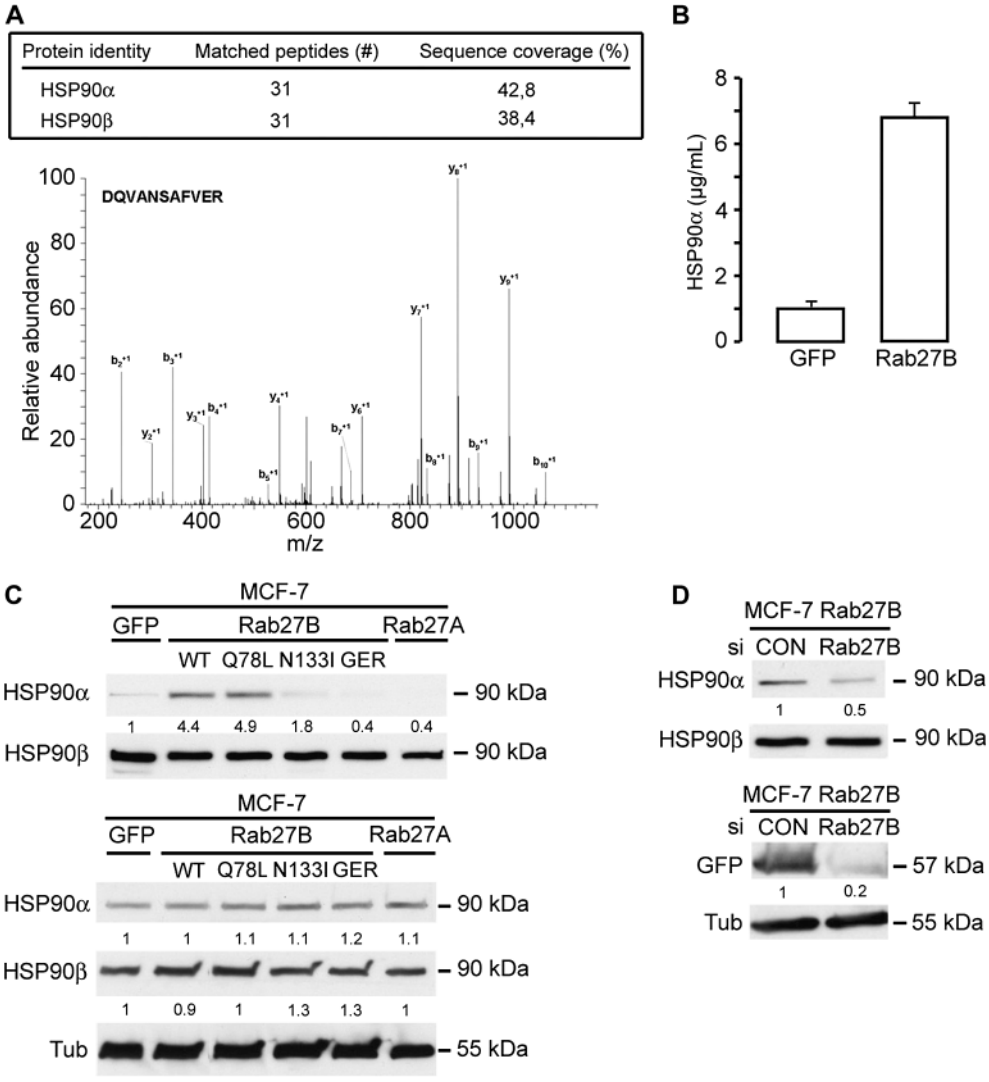

Figure 4. Selective stimulation of heat-shock protein (HSP)90α secretion by Rab27B through GTP- and geranylgeranyl-dependent mechanisms. **A**) Secretome profiling of invasive MCF-7 green fluorescent protein (GFP)-Rab27B cancer cells identified HSP90α and HSP90β. The number of matched peptides and the percentage of sequence coverage are indicated for both proteins. The mass spectrometry/mass spectrometry spectrum recorded on a $[M+2H]^{2+}$ ion at m/z 618.69 corresponds to a unique peptide [DQVANSAFVER], derived from HSP90α. Peptides fragment along the amide backbone to produce sequence-specific fragment ions; ions containing the C-terminal fragment are known as "y" ions, whereas ions containing the N-terminal fragment are known as "b" ions. The search engine Mascot uses this information to report probability-based scores for each peptide. See "Materials and Methods" for more details. **B**) Quantification of HSP90α levels in conditioned medium (CM) of GFP- vs GFP-Rab27B-expressing (wild type, WT) MCF-7 cells using enzyme-linked immunosorbent assay. Results are means with upper 95% confidence intervals of two independent experiments with three replicates. **C**) Western blot analysis of HSP90α and HSP90β in CM (**upper panel**) and in total protein lysates (**lower panel**) of transfected MCF-7 cells. Relative intensity was quantified with HSP90β or tubulin as a loading control. **D**) Impact of Rab27B silencing (siRab27B-1 and -2) vs control silencing (siCON) on the expression of GFP-Rab27B protein (**lower panel**) and secretion of HSP90α and HSP90β (**upper panel**) in the CM of MCF-7 GFP-Rab27B cells. Protein levels were quantified as immunostaining intensity relative to tubulin and HSP90β, respectively.

In additional experiments, we examined the ability of HSP90 or its inhibitors to affect invasive growth. We first explored the ability of 1 μM concentrations of an HSP90 inhibitor, geldanamycin, or its derivative, 17-AAG (39), to reverse the invasive potential of MCF-7 GFP-Rab27B cells in the type I collagen invasion assay described previously. Each of these drugs was able to inhibit invasion by 85% ($P < .001$) (Figure 5, A) at this concentration, and less than 1% toxicity was observed in Trypan blue exclusion assays. Geldanamycin and 17-AAG are able to inhibit both secreted and intracellular HSP90α and HSP90β. Therefore, to determine whether invasion could be inhibited by reducing only extracellular HSP90 activity, we also tested the effect of an anti-HSP90α–specific neutralizing antibody, which reversed the invasive phenotype of MCF-7 GFP-Rab27B cells by 4.3-fold ($P < .001$) (Figure 5, B). Finally, we examined whether addition of HSP90 to the cell culture medium could promote invasion. We observed a dose-dependent increase in type I collagen invasion by MCF-7 cells treated with 1–10 μg/mL recombinant HSP90α ($P = .04$ at 5 μg/mL, and $P = .003$ at 10 μg/mL, χ^2 test) (Figure 5, C); however, addition of 10 μg/mL recombinant HSP90β had no effect.

Next, we examined the role of HSP90α in Rab27B-induced proliferation and Rab27B-increased cyclin A expression. The anti-HSP90α–specific neutralizing antibody (5 μg/mL) reversed the increased proliferation of MCF-7 GFP-Rab27B cells by fivefold ($P < .001$) (Figure 5, D) and inhibited cyclin A expression by twofold (Figure 5, E). In accordance, we observed increased proliferation of MCF-7 cells upon addition of 10 μg/mL recombinant HSP90α to the culture medium ($P < .001$) (Figure 5, D) and increased cyclin A expression (Figure 5, E) at a 10 μg/mL concentration that was similar to that found in the secretome of Rab27B-overexpressing cells.

What is the molecular mechanism of HSP90α in promoting invasive growth? It is known that HSP90α serves as an extracellular chaperone for MMP-2, a protease that degrades extracellular matrix (38); the active form is 68 kDa, produced by cleavage of a peptide from the 72-kDa pro-protein. Extracellular 68 kDa MMP-2 activity increased 2.1-fold in MCF-7 cells transfected with GFP-Rab27B and 5.3-fold in MCF-7 cells expressing constitutively active GFP-Rab27B-Q78L but was decreased in MCF-7 variants transfected with the dominant negative or geranylgeranyl

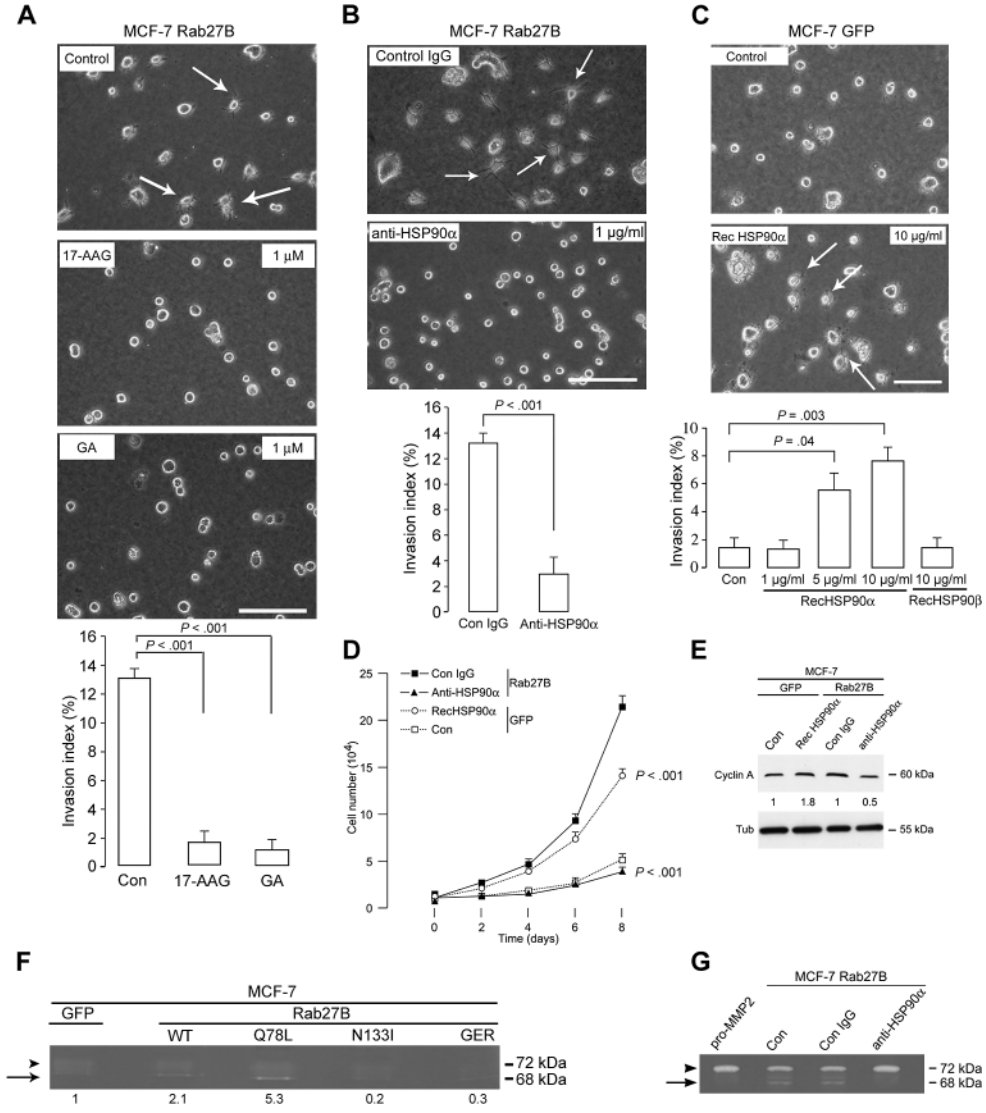

Figure 5. The role of heat-shock protein (HSP)90α and matrix metalloproteinase (MMP)-2 in Rab27B-dependent invasion. **A**) Phase-contrast images showing morphology (**upper panels**) and quantification of collagen type I invasion by MCF-7 green fluorescent protein (GFP)-Rab27B cells (**lower panel**) treated with the HSP90α inhibitors 17-(allylamino)-17-demethoxygeldanamycin (17-AAG) and geldanamycin (GA) (1 μM) for 24 hours or left untreated (Control, Con). **B**) Morphology (**upper panels**) and quantification (**lower panel**) of the invasive phenotype induced by GFP-Rab27B in MCF-7 cells cultured on collagen type I matrix treated for 6 hours with HSP90α neutralizing antibody (1 μg/mL) or the control IgG isotype. **C**) Morphology (**upper panel**) and quantification (**lower panel**) of the invasive phenotype induced by HSP90 in MCF-7 GFP cells cultured on collagen type I matrix and treated for 24 hours in the presence or absence (Control, Con) of recombinant (rec) HSP90α protein (1, 5, and 10 μg/mL) or recombinant HSP90β protein (10 μg/mL). In (**A**), (**B**), and (**C**), **arrows** indicate cellular extensions and local spreading. Scale bar, 100 μm. Invasion indices are means and upper 95% confidence intervals derived from the means of three independent experiments performed in triplicate. *P* values are calculated using the χ^2 test; statistically significant *P* values are indicated. **D**) Measurement of cell proliferation rates of MCF-7 GFP cells treated with recombinant HSP90α (10 μg/mL) or left untreated (Con) and of MCF-7 GFP-Rab27B cells challenged with a HSP90α neutralizing antibody (5 μg/mL) or control immunoglobulin (Con IgG). Proliferation assay was performed as in Figure 2, G. Mean number of cells is plotted with upper 95% confidence intervals. *P* values are calculated using the two-way repeated measures analysis of variance test. **E**) Cyclin A expression was evaluated in MCF-7 GFP cells treated with recombinant HSP90α (10μg/mL) or left untreated (Con) and in MCF-7 GFP-Rab27B cells challenged with HSP90α neutralizing or control antibody. Intensity was quantified relative to tubulin. **F**) Analysis of MMP-2 activity in conditioned medium (CM) from cultured MCF-7 cells expressing GFP, GFP-Rab27B (wild type, WT), or the GFP-Rab27B mutants (Q78L, N133I, and GER) by gelatin zymography. **G**) Gelatin zymography of MMP-2 activity in CM from MCF-7 GFP-Rab27B cells that were preincubated with exogenously added proMMP-2 (100 ng/mL) in serum-free medium for 24 hours. In (**F**) and (**G**), **arrowhead** indicates 72 kDa proMMP-2 and **arrow** indicates 68 kDa active protease.

mutants of Rab27B (Figure 5, F). In agreement, recombinant proMMP-2 that was exogenously added to MCF-7 GFP-Rab27B cells was activated in an HSP90α-dependent manner as demonstrated by the inhibitory effects of the specific anti-HSP90α neutralizing antibody (Figure 5, G).

Expression of Rab27B in Primary Human Breast Tumors

We next analyzed the expression of the Rab27B protein in 59 primary breast tumors by IHC using our Rab27B-specific antibody (Figure 6, A and B, and Supplementary Table 2, available online). Breast tumors with no or weak cytoplasmic Rab27B expression and with less than 5% of cancer cells showing membrane localization and/or vesicle clustering, that is, score = 0, were ER negative (10 of 10, 100%), whereas tumors with cytoplasmic Rab27B distribution and prominent membrane localization and/or vesicle clustering, that is, a score 1 or 2, were ER positive (49 of 49, 100%; $P < .001$). Conversely, ER status was perfectly associated with Rab27B status. Furthermore, there was a statistically significant association between Rab27B score 2 (>30% of cancer cells showing prominent Rab27B localization at the plasma membrane or vesicle clusters) and positive lymph node metastases ($P < .001$) as well as tumor grade ($P = .001$) (Figure 6, B). Lysates from MCF-7 GFP-Rab27B cells or from epithelial tissues microdissected from fresh-frozen primary human breast cancer tissue with immunohistochemical scores of 0, 1, or 2 were subjected to western blotting with our Rab27B-specific polyclonal antibody. Similar Rab27B expression levels were observed in MCF-7 cells that stably expressed ectopic GFP-Rab27B and in microdissected breast tissue with an IHC score of 2 (that tended to metastasize more frequently to the lymph nodes) (Supplementary Figure 5, available online). Endogenous Rab27B levels in noninvasive MCF-7 cells had expression levels similar to those in microdissected breast tissue with an IHC score

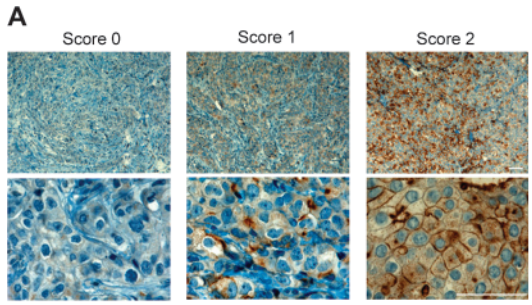

B

Variable	Score 0	Score 1	Score 2	
Total No. of patients	10	32	17	
ER status				$P < .001$
Negative	10	0	0	
Positive	0	32	17	
Node status				$P < .001$
Negative	2	23	4	
Positive	8	7	13	
Grade				$P = .001$
I	0	2	0	
II	0	17	3	
III	9	7	9	

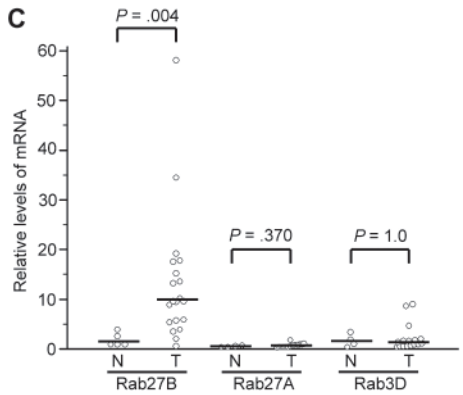

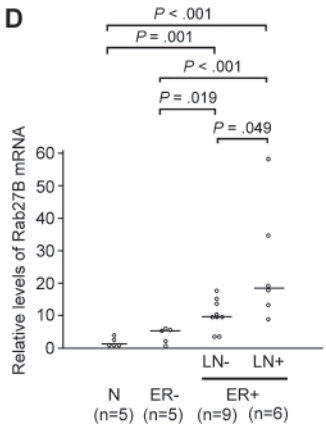

Figure 6. Rab27B expression in clinical breast cancer specimens. **A**) Representative Rab27B stained primary breast cancer samples that illustrate immunohistochemical scores of 0, 1, and 2. Scale bar, 100 μm. **B**) Associations of Rab27B immunohistochemical scores with estrogen receptor (ER) status and other clinicopathological data for 59 primary breast tumors. The χ^2 test was used to test for differences between categorical variables. **C**) Relative levels of Rab3D, Rab27A, and Rab27B mRNA expression in normal tissue (N, n = 5) vs primary breast carcinoma (T, n = 20). **D**) Expression of Rab27B mRNA in five normal tissues vs 20 primary breast carcinomas. Tumor samples were divided into three groups according to ER status and lymph node (LN) involvement. In (**C**) and (**D**), mRNA expression was measured by quantitative real-time polymerase chain reaction in triplicate. **Horizontal bars** represent median for each group (two-sided Mann–Whitney test).

of 1 (that had a less aggressive character); ER-negative breast tumors did not express Rab27B (Supplementary Figure 5, available online).

We next investigated the relative expression of Rab3D, Rab27A, and Rab27B mRNAs in 20 tumor samples by quantitative real-time PCR. Median expression of Rab3D and Rab27A did not statistically significantly differ between normal and tumor tissue ($P = 1.0$ and $P = .37$, respectively) (Figure 6, C). By contrast, median expression of Rab27B was 10-fold higher in tumor tissue compared with normal tissue ($P = .004$, Mann–Whitney test). To investigate the relationship between Rab27B mRNA expression and clinical parameters, the 20 tumor samples were divided into two groups according to ER status (Figure 6, D). As might be predicted from our previous IHC results, Rab27B mRNA expression levels statistically significantly differed between ER-negative vs ER-positive tumor samples ($P = .019$ and $P < .001$), whereas no statistically significant difference was observed between normal samples and ER-negative tumors ($P = .22$). In addition, the median accumulation of Rab27B mRNA was twofold higher in the ER-positive group of patients with lymph node metastases compared with those without lymph node metastases ($P = .049$) (Figure 6, D). On 17 of the 20 tumor samples, we performed both quantitative real-time PCR and IHC and demonstrated that in 14 (82%) of the 17 samples analyzed, Rab27B mRNA expression strictly followed protein expression. We performed fluorescence in situ hybridization analysis on 10 tumor samples randomly selected among the 17 tumor samples that had an immunohistochemical score of 2, but this test revealed no amplification of the *RAB27B* gene (Supplementary Table 2, available online).

Discussion

Known hallmarks of malignancy include defective vesicular trafficking of growth factor receptors and unbalanced recycling of integrin- and cadherin-based adhesion complexes (40). In this article, we have identified a new key mechanism that links the secretory small GTPase Rab27B with HSP90α secretion leading to MMP-2 stabilization, activation, and cancer cell invasion. We demonstrate that in ER-positive human breast cancer cells, the Rab27B-regulated secretory pathway delivers proinvasive signals involved in the degradation of extracellular matrix components. In addition to promoting reorganization of the actin cytoskeleton, Rab27B also induces G_1 to S cell cycle progression and cellular proliferation (Figure 2). Rab27B promotes the invasive growth of primary tumors and the multiplication of peritoneal metastases established from MCF-7 human breast cancer xenografts (Figure 3). The functional impact of the Rab27B small GTPase in vitro and in vivo

depends exclusively upon lipid targeting (ie, geranylgeranylation) and GTP binding (Figures 2 and 3).

Human Rab27A and Rab27B are structurally very similar and are functional homologs with respect to melanosome transport (29). However, the functions of the A and B isoforms are not always redundant, as shown by the distinct roles of Rab27A and Rab27B in granule exocytosis in human neutrophils and mouse bone marrow–derived mast cells (41,42). Recently, Wang et al. (25) showed that increased expression of Rab27A further enhances the already established invasive and metastatic phenotypes of the ER-negative human breast cancer cell lines MDA-MB-231 and MDA-MB-435 (28). In these models, Rab27A had a perinuclear and non-cytoskeleton–associated localization pattern, suggesting a nonsecretory function for Rab27A in MDA-MB cell lines (25). The invasive potential of Rab27A in MCF-7 cells and the role of WT Rab27B and its GTP-binding mutants were not explored (25).

How does Rab27B achieve invasive growth? Proteomic analysis of purified GFP-Rab27B vesicles and of the secretome of MCF-7 GFP-Rab27B identified HSP90α as a potential proinvasive growth regulator. Extracellular HSP90α was already known to stimulate keratinocyte migration (43), wound healing (44), and cancer cell invasion (38). Our data show that intracellular HSP90α, but not β, is secreted into the extracellular environment in a Rab27B-specific, GTP-dependent, and geranylgeranyl-dependent manner (Figure 4, A–C). Consistent with this finding, the use of siRNAs targeting Rab27B in addition to HSP90α neutralizing antibodies, pharmacological inhibitors, and recombinant HSP90 proteins demonstrated the critical role for Rab27B and HSP90α in enhancing breast cancer cell invasion and proliferation (Figures 4, D, and 5, A–E).

Elucidation of the clientele of receptors, growth factors, and proteases that is regulated by extracellular HSP90α and of how this molecule functions extracellularly in stimulating invasive growth comprises a very ambitious goal. We cannot rule out a combination of mechanisms that includes the stabilization of interactions by growth factors with the extracellular domains of growth factor receptors (45). One reported client protein is MMP-2, a protease that requires association with extracellular HSP90α for its activity (38,46). A well-characterized property of invasive cancer cells is their ability to accelerate the degradation of extracellular matrix by MMPs and to release and activate growth factors (47,48).

MMPs show increased expression and activation in almost all human cancers with poor clinical prognoses (49). MMPs are attractive cancer targets, but clinical trials of broad-spectrum MMP inhibitors have failed to establish increased patient survival (50). This brings to question the adequacy of attempts to develop MMPs as drug targets, which may have failed because MMP inhibitors advanced to clinical trials without adequate understanding of MMP activation cascades (49). Pro-MMPs are secreted, chaperoned, and activated extracellularly by proteolytic digestion of the inhibitory propeptide domain. Excessive extracellular MMP activation in cancers with poor clinical prognosis may require specific chaperoning functions that are not required by normal physiology. Extracellular chaperoning could open a new window for future targeting of MMP activation. We verified that MMP-2 activation depends on extracellular HSP90α chaperoning and showed that it is associated with Rab27B activity; interestingly, we found no such regulation for MMP-9 (Figure 5, F and G, and data not shown). One possible explanation is that extracellular HSP90α clients, among them MMP-2, confer to cells a gain in matrix degradation and growth factor activation leading to increased invasive growth.

It is known that elevated expression of intra- and extracellular HSP90α predicts decreased survival in various cancers (51,52). Specifically, in ER-positive breast tumors, HSP90 expression was associated with lymph node metastasis and decreased survival; however, these authors did not distinguish between HSP90α and HSP90β (53). It is not surprising that HSP90 has been suggested as a promising target for the treatment of various cancers and that clinical phase I and phase II trials are ongoing (54). Nevertheless, caution is needed because this molecular chaperone assists in the cellular function of many client proteins involved in physiology and malignancy. Targeting extracellular and cell surface HSP90α will not affect the stability of intracellular client proteins. Recently, a cell-impermeable HSP90α inhibitor was shown to affect F-actin organization and inhibited metastatic growth in a mouse melanoma model (55). Hyperacetylation of extracellular HSP90α, involved in MMP-2 chaperoning and activation, may add further target specificity as demonstrated by treatment with an anti-acetyl lysine-69 HSP90α antibody in a cell culture breast cancer invasion model (46). Future experiments should reveal whether Rab27B is implicated in secretion of the hyperacetylated HSP90α.

ER-positive breast cancers, which comprise the majority of breast malignancies, carry a better prognosis for disease-free survival and overall survival than ER-negative breast cancers (56). Nevertheless, some ER-positive breast cancers are more invasive and tend to metastasize more frequently than other ER-positive tumors. A low degree of differentiation and the presence of metastasis in the axillary lymph nodes are typical characteristics. The underlying reasons for the more aggressive character are poorly understood (56).

In this study, Rab27B expression was identified as a key factor for the increased invasiveness, tumor size, and metastasis of various ER-positive breast cancer cell lines, both in vitro and in vivo. Critically, in human breast cancer specimens, the presence of Rab27B protein proved to be associated with a low degree of differentiation, presence of lymph node metastasis, and a positive ER status (Figure 6, A and B). In agreement, levels of Rab27B mRNA were highest in ER-positive breast cancers with lymph node metastasis and lowest in ER-negative tumors (Figure 6, D). Also, during the course of our experiments, Wright et al. (57) found higher mean Rab27B mRNA levels in ER-positive than in ER-negative invasive breast carcinoma tissues. The molecular and biological relevance of our data is further supported by the similarity of the Rab27B expression level and localization pattern in breast cancer cell lines expressing ectopic GFP-Rab27B, their primary xenografts, and patient-derived breast cancer tissue. Based on this body of evidence, Rab27B is as a major effector of invasiveness and metastasis and provides an important marker in the signature of ER-positive breast cancers with poor prognosis.

The study has several potential limitations. One is the use of immunocompromised mice as preclinical models of human malignancies. Xenografts do not always reflect the heterogeneity and complexity seen in human tumors. Furthermore, tumor growth in athymic mice may not necessarily recapitulate the pattern of tumor

growth that occurs in humans because of immune surveillances. The xenograft model could be extended by studies of spontaneous or transgenic models of breast cancer. Second, our study could be strengthened if invasive and ER-positive breast cancer cell lines were available in the scientific community: to our knowledge, there are none. These cell lines would be very useful to check endogenous Rab27B levels and to target it by siRNA treatment. Third, our study did not explain in detail how Rab27B-dependent secretion of HSP90α is mechanistically implicated in invasive growth. Although we could confirm the results obtained by Eustace et al. (38) and Yang et al. (46), that showed the importance of extracellular HSP90α in the activation of MMP-2; we do not have evidence of whether MMP-2 is necessary and sufficient for the invasive growth mechanisms induced by Rab27B (38,46). Therefore, we cannot rule out the possibility that a combination of extracellular substrates might be important for the Rab27B-dependent invasive growth program.

In conclusion, dysregulation of Rab27B expression might prove to be a generalized feature of human tumors. Considerable therapeutic potential may reside in efforts to control Rab27B levels and to modulate Rab27B-regulated pathways through pharmacological or genetic interventions.

Supplementary Data

Supplementary data can be found at http://www.jnci.oxfordjournals.org/.

References

1. Comoglio PM, Trusolino L. Invasive growth: from development to metastasis. *J Clin Invest.* 2002;109(7):857–862.
2. Palmer RE, Lee SB, Wong JC, et al. Induction of BAIAP3 by the EWS-WT1 chimeric fusion implicates regulated exocytosis in tumorigenesis. *Cancer Cell.* 2002;2(6):497–505.
3. Pereira-Leal JB, Seabra MC. Evolution of the Rab family of small GTP-binding proteins. *J Mol Biol.* 2001;313(4):889–901.
4. Zerial M, McBride H. Rab proteins as membrane organizers. *Nat Rev Mol Cell Biol.* 2001;2(3):107–117.
5. Vetter IR, Wittinghofer A. The guanine nucleotide-binding switch in three dimensions. *Science.* 2001;294(5545):1299–1304.
6. Pfeffer SR. Structural clues to Rab GTPase functional diversity. *J Biol Chem.* 2005;280(16):15485–15488.
7. Leung KF, Baron R, Seabra MC. Thematic review series: lipid posttranslational modifications. Geranylgeranylation of Rab GTPases. *J Lipid Res.* 2006;47(3):467–475.
8. Burgess TL, Kelly RB. Constitutive and regulated secretion of proteins. *Annu Rev Cell Biol.* 1987;3:243–293.
9. Chavez RA, Miller SG, Moore H-PH. A biosynthetic regulated secretory pathway in constitutive secretory cells. *J Cell Biol.* 1996;133(6):1177–1191.
10. Burgoyne RD, Morgan A. Secretory granule exocytosis. *Physiol Rev.* 2003;83(2):581–632.
11. Fukuda M. Regulation of secretory vesicle traffic by Rab small GTPases. *Cell Mol Life Sci.* 2008;65(18):2801–2813.
12. Nashida T, Imai A, Shimomura H. Relation of Rab26 to the amylase release from rat parotid acinar cells. *Arch Oral Biol.* 2006;51(2):89–95.
13. Masuda ES, Luo Y, Young C, et al. Rab37 is a novel mast cell specific GTPase localized to secretory granules. *FEBS Lett.* 2000;470(1):61–64.
14. Takai Y, Sasaki T, Shirataki H, Nakanishi H. Rab3A small GTP-binding protein in Ca(2+)-dependent exocytosis. *Genes Cells.* 1996;1(7):615–632.
15. Gomi H, Mori K, Itohara S, Izumi T. Rab27b is expressed in a wide range of exocytic cells and involved in the delivery of secretory granules near the plasma membrane. *Mol Biol Cell.* 2007;18(11):4377–4386.
16. Tolmachova T, Anders R, Stinchcombe J, et al. A general role for Rab27a in secretory cells. *Mol Biol Cell.* 2004;15(1):332–344.
17. Riedel D, Antonin W, Fernandez-Chacon R, et al. Rab3D is not required for exocrine exocytosis but for maintenance of normally sized secretory granules. *Mol Cell Biol.* 2002;22(18):6487–6497.
18. Chen D, Guo J, Miki T, Tachibana M, Gahl WA. Molecular cloning and characterization of rab27a and rab27b, novel human rab proteins shared by melanocytes and platelets. *Biochem Mol Med.* 1997;60(1):27–37.
19. Cheng KW, Lahad JP, Kuo W-L, et al. The RAB25 small GTPase determines aggressiveness of ovarian and breast cancers. *Nat Med.* 2004;10(11):1251–1256.
20. Kanda I, Nishimura N, Nakatsuji H, et al. Involvement of Rab13 and JRAB/MICAL-L2 in epithelial cell scattering. *Oncogene.* 2008;27(12):1687–1695.
21. Liu Y-J, Wang Q, Li W, et al. Rab23 is a potential biological target for treating hepatocellular carcinoma. *World J Gastroenterol.* 2007;13(7):1010–1017.
22. Hou Q, Wu YH, Grabsch H, et al. Integrative genomics identifies RAB23 as an invasion mediator gene in diffuse-type gastric cancer. *Cancer Res.* 2008;68(12):4623–4630.
23. Fukui K, Tamura S, Wada A, et al. Expression of Rab5a in hepatocellular carcinoma: possible involvement in epidermal growth factor signaling. *Hepatol Res.* 2007;37(11):957–965.
24. Bravo-Cordero JJ, Marrero-Diaz R, Megías D, et al. MT1-MMP proinvasive activity is regulated by a novel Rab8-dependent exocytic pathway. *EMBO J.* 2007;26(6):1499–1510.
25. Wang J-S, Wang F-B, Zhang Q-G, Shen Z-Z, Shao Z- M. Enhanced expression of Rab27A gene by breast cancer cells promoting invasiveness and the metastasis potential by secretion of insulin-like growth factor-II. *Mol Cancer Res.* 2008;6(3):372–382.
26. Chia WJ, Tang BL. Emerging roles for Rab family GTPases in cancer. *Biochim Biophys Acta.* 2009;1795(2):110–116.
27. Dobashi S, Katagiri T, Hirota E, et al. Involvement of TMEM22 overexpression in the growth of renal cell carcinoma cells. *Oncol Rep.* 2009;21(2):305–312.
28. Neve RM, Chin K, Fridlyand J, et al. A collection of breast cancer cell lines for the study of functionally distinct cancer subtypes. *Cancer Cell.* 2006;10(6):515–527.
29. Westbroek W, Lambert J, De Schepper S, et al. Rab27b is up-regulated in human Griscelli syndrome type II melanocytes and linked to the actin cytoskeleton via exon F-Myosin Va transcripts. *Pigment Cell Res.* 2004;17(5):498–505.
30. Westbroek W, Tuchman M, Tinloy B, et al. A novel missense mutation (G43S) in the switch I region of Rab27A causing Griscelli syndrome. *Mol Genet Metab.* 2008;94(2):258–254.
31. Barral DC, Ramalho JS, Anders R, et al. Functional redundancy of Rab27 proteins and the pathogenesis of Griscelli syndrome. *J Clin Invest.* 2002;110(2):247–257.
32. De Wever O, Hendrix A, De Boeck A, et al. Modeling and quantification of cancer cell invasion through collagen type I matrices. *Int J Dev Biol.* 2009. doi: 10.1387/ijdb.092948ow.
33. De Wever O, Nguyen Q-D, Van Hoorde L, et al. Tenascin-C and SF/HGF produced by myofibroblasts in vitro provide convergent pro-invasive signals to human colon cancer cells through RhoA and Rac. *FASEB J.* 2004;18(9):1016–1018.
34. Maynard DM, Heijnen HFG, Horne MK, White JG, Gahl WA. Proteomic analysis of platelet α-granules using mass spectrometry. *J Thromb Haemost.* 2007;5(9):1945–1955.
35. Perkins DN, Pappin DJ, Creasy DM, Cottrell JS. Probability-based protein identification by searching sequence databases using mass spectrometry data. *Electrophoresis.* 1999;20(18):3551–3567.
36. Huang DW, Sherman BT, Lempicki RA. Systematic and integrative analysis of large gene lists using DAVID bioinformatics resources. *Nat Protoc.* 2009;4(1):44–57.
37. McNeill RE, Miller N, Kerin MJ. Evaluation and validation of candidate endogenous control genes for real-time quantitative PCR studies of breast cancer. *BMC Mol Biol.* 2007;8:107.
38. Eustace BK, Sakurai T, Stewart JK, et al. Functional proteomic screens reveal an essential extracellular role for hsp90α in cancer cell invasiveness. *Nat Cell Biol.* 2004;6(6):507–514.

39. Sharp S, Workman P. Inhibitors of the HSP90 molecular chaperone: current status. *Adv Cancer Res.* 2006;95:323–348.
40. Mosesson Y, Mills GB, Yarden Y. Derailed endocytosis: an emerging feature of cancer. *Nat Rev Cancer.* 2008;8(11):835–850.
41. Herrero-Turrión MJ, Calafat J, Janssen H, Fukuda M, Mollinedo F. Rab27a regulates exocytosis of tertiary and specific granules in human neutrophils. *J Immunol.* 2008;181(6):3793–3803.
42. Mizuno K, Tolmachova T, Ushakov DS, et al. Rab27b regulates mast cell granule dynamics and secretion. *Traffic.* 2007;8(7):883–892.
43. Li W, Li Y, Guan S, et al. Extracellular heat shock protein-90α: linking hypoxia to skin cell motility and wound healing. *EMBO J.* 2007; 26(5):1221–1233.
44. Cheng C-F, Fan J, Fedesco M, et al. Transforming growth factor α (TGFα)-stimulated secretion of HSP90α: using the receptor LRP-1/ CD91 to promote human skin cell migration against a TGFβ-rich environment during wound healing. *Mol Cell Biol.* 2008;28(10): 3344–3358.
45. Sidera K, Gaitanou M, Stellas M, Matsas R, Patsavoudi E. A critical role for HSP90 in cancer cell invasion involves interaction with the extracellular domain of HER-2. *J Biol Chem.* 2008;283(4):2031–2041.
46. Yang Y, Rao R, Shen J, et al. Role of acetylation and extracellular location of heat shock protein 90α in tumor cell invasion. *Cancer Res.* 2008; 68(12):4833–4842.
47. Friedl P, Gilmour D. Collective cell migration in morphogenesis, regeneration and cancer. *Nat Rev Mol Cell Biol.* 2009;10(7):445–457.
48. Page-McCaw A, Ewald AJ, Werb Z. Matrix metalloproteinases and the regulation of tissue remodeling. *Nat Rev Mol Cell Biol.* 2007;8(3): 221–233.
49. Overall CM, Kleifeld O. Validating matrix metalloproteinases as drug targets and anti-targets for cancer therapy. *Nat Rev Cancer.* 2006;6(3): 227–239.
50. Coussens LM, Fingleton B, Matrisian LM. Matrix metalloproteinase inhibitors and cancer: trials and tribulations. *Science.* 2002;295(5564): 2387–2392.
51. Li C-F, Huang W-W, Wu J-M, et al. Heat shock protein 90 overexpression independently predicts inferior disease-free survival with differential expression of the α and β isoforms in gastrointestinal stromal tumors. *Clin Cancer Res.* 2008;14(23):7822–7831.
52. Xu A, Tian T, Hao J, et al. Elevation of serum HSP90α correlated with the clinical stage of non-small cell lung cancer. *J Cancer Mol.* 2007;3(4): 107–112.
53. Pick E, Kluger Y, Giltnane JM, et al. High HSP90 expression is associated with decreased survival in breast cancer. *Cancer Res.* 2007;67(7):2932–2937.
54. Banerji U. Heat shock protein 90 as a drug target: some like it hot. *Clin Cancer Res.* 2009;15(1):9–14.
55. Tsutsumi S, Scroggins B, Koga F, et al. A small molecule cell-impermeant HSP90 antagonist inhibits tumor cell motility and invasion. *Oncogene.* 2008;27(17):2478–2487.
56. Pagani O, Price KN, Gelber RD, et al. Patterns of recurrence of early breast cancer according to estrogen receptor status: a therapeutic target for a quarter of a century. *Breast Cancer Res Treat.* 2009;117(2):319–324.
57. Wright PK, May FEB, Darby S, et al. Estrogen regulates vesicle trafficking gene expression in EFF-3, EFM-19 and MCF-7 breast cancer cells. *Int J Clin Exp Pathol.* 2009;2(5):463–475.

Funding

Intramural Research Program of the National Human Genome Research Institute, "Centrum voor gezwelziekten," Institut National de la Santé et de la Recherche Médicale, Association pour la Recherche sur le Cancer, the Scientific Exchange Program between the Flemish community and France (I.2007.03, T.2009.14), European Association for Cancer Research (to A.H. and O.D.W.) and Journal of Cell Science (to O.D.W.) travel fellowships and a travel grant (A.H. and O.D.W.) and postdoctoral grant (O.D.W.) from Fund for Scientific Research-Flanders.

Notes

W. Westbroek and O. De Wever contributed equally to this work.

The study sponsors have no role in the design of the study; the collection, analysis, and interpretation of the data; the writing of the manuscript; or the decision to submit the manuscript for publication.

M. Mareel is gratefully acknowledged for stimulating discussions. We thank G. De Bruyne, A. Verspeelt, M. De Meulemeester, S. Decloedt, K. Lambein, and S. Geenen for excellent technical assistance. We are grateful to M. Kirby and S. Anderson (National Human Genome Research Institute Flow Cytometry Core, National Institutes of Health) for support with the vesicle isolation.

Affiliations of authors: Medical Genetics Branch, National Human Genome Research Institute, Bethesda, MD (DM, WAG, WW); Department of Medical Oncology (AH, HD, SVB, VC), Laboratory of Experimental Cancer Research (MB, ODW), Department of Pathology (PP), Department of Gynecology (GB, RVdB), and Department of Dermatology (JL), Ghent University Hospital, Ghent, Belgium; INSERM U673 Molecular and Clinical Oncology of Solid Tumors, Paris, France (CG); INSERM U938, Paris, France (CG); Université Pierre et Marie Curie-Paris 6, Faculté de Médecine, Paris cedex 12, France (CG); Molecular Medicine, National Heart and Lung Institute, Imperial College London, London, UK (MCS); CEDOC, Faculdade de Ciências Médicas, Universidade Nova de Lisboa, Lisbon, Portugal (MCS); Instituto Gulbenkian de Ciência, Oeiras, Portugal (MCS).